Stability of naturally occurring AMD–schwertmannite in the presence of arsenic and reducing agents

JUAN ANTELO[1,*], SARAH FIOL[1,2], IVAN CARABANTE[3,4], ARANTXA ARROYO[2], JUAN S. LEZAMA-PACHECO[4], NATASHA JOSEVSKA[3], CHLOE PROTOPAPA[3], JURATE KUMPIENE[3]

[1]CRETUS-Institute, Cross-disciplinary Research in Environmental Technologies. University of Santiago de Compostela, 15782 Santiago de Compostela, Spain

[2]Department of Physical Chemistry, University of Santiago de Compostela, 15782 Santiago de Compostela, Spain

[3]Waste Science and Technology, Department of Civil, Mining & Environmental Engineering, Luleå University of Technology, SE-97187 Luleå, Sweden

[4]Department of Earth System Science, School of Earth, Energy, and Environmental Sciences, Stanford University, Stanford, CA 94305, USA

[*]**Corresponding Author**: juan.antelo@usc.es

Highlights

- Secondary iron precipitates from AMD are efficient scavengers of metal(loids)
- Ion exchange was found to be a key mechanism in the accumulation of metal(loids)
- Metal(oids) stabilized secondary iron minerals, delaying the remobilization processes
- The use of XRD and XAS was crucial to understand mineral transformation processes
- pH, redox and metal(loids) are key factors in the long-term stability of AMD minerals

Abstract

Secondary iron oxides formed in acid mine drainage, such as schwertmannite, are scavengers for metal(loid)s in mining environments. Increasing the understanding of the geochemical transformations of these minerals, as well as knowing how metal(loid)s affect these transformations, is crucial to ultimately predict the fate of these trace elements in acidic mine drainage and to minimize the potential environmental risk. In this study, transformation experiments have been conducted with a schwertmannite-rich sediment collected from a mining area and with synthesized schwermannite as a reference material. The transformation of schwertmannite into goethite was studied as a function of the presence of arsenic, pH value, and redox conditions. Arsenic delayed the mineral transformation from pseudo-stable amorphous phases to more stable crystalline forms, especially at higher arsenic loadings and more acidic pH. Experiments in the presence of Fe(II) and ascorbic acid have proven that both components promote the mineral transformation or reductive dissolution of schwertmannite under anoxic conditions. The presence of arsenic reduced the catalytic effect of Fe(II), stabilizing the schwertmannite particles. On the other hand, arsenic had no effect on the reductive dissolution at these conditions when ascorbic acid was used as a reducing agent.

Keywords: acid mine drainage; schwertmannite, goethite, arsenic, mineral stability, oxic and anoxic conditions

1. Introduction

Contamination of soils and aqueous systems affected by acid mine drainage (AMD) is a serious threat that demands the attention of the scientific community (Moodley et al., 2018). Among the environmental risks derived from AMD, the extremely low pH of affected waters, the high concentration of sulphate and heavy metals either dissolved or accumulated in adjacent soils or the impact on the local flora and fauna, can be mentioned. In anoxic environments, Fe-S biogeochemistry can control trace metals and metal(loid)s bioavailability and acidity generation. However, sulphide minerals undergo oxidation upon exposure to air following natural weathering processes and anthropogenic activities (Karimian et al., 2018). This oxidation process leads to the formation of large amounts of iron and aluminium secondary minerals, which determines the mobility of trace elements in AMD systems. Although iron (hydr)oxides have been part of the problem, due to their natural presence and transformation in mining areas generating extreme acidity in soils and streams upon sulfides oxidation, they are also known to be part of the solution due to their implication in natural attenuation processes (Asta et al., 2010; Carlson et al., 2003). This natural ability of iron minerals has been considered in the elaboration of some recent remediation techniques, such as Technosols, which may contain acid mine water or mining sediments in their composition along with other agro-industrial wastes (Arán et al., 2018). The accumulation of trace elements by iron and aluminium secondary precipitates have thus the advantage that toxic elements are immobilised in the sediments and therefore the risk associated to the spreading of these elements into the environment is reduced. Another advantage of the accumulation of trace elements by secondary precipitates could be the possibility to recover valuable elements, such as Rear Earth Elements (REE) which are defined as critical raw materials. REE are present in AMD sites in several orders of magnitude higher than in natural environments due to their affinity to schwertmannite and basaluminite (Lozano et al., 2019; Lozano et al., 2020).

In this sense, the role of iron precipitates formed in AMD has been studied from the microscopic and macroscopic points of view (Antelo et al., 2013; Asta et al., 2010; Baleeiro et al., 2018; Jönsson et al., 2006) to assess their potential use by exploiting their sequestration or immobilisation properties. The pH, along with time, temperature, composition of the solid and aqueous phases and oxidizing capacity of the medium, are key factors that determine the type of iron mineral that is formed in AMD affected areas (Nordstrom and Alpers, 1999; Bigham and Nordstrom, 2000). Whereas amorphous pseudo-stable phases, schwertmannite and ferrihydrite, precipitate in the lower pH range, 2.8-6.5, crystalline, thermodynamically stable phases such as goethite are formed at pH > 6.5.

Schwertmannite, typically formed in AMD environments, can remain stable for years under acidic conditions (Regenspurg et al., 2004), although it tends to transform into goethite depending on the environmental conditions, being the pH an important factor (Antelo et al., 2013; Kumpulainen et al., 2008; Parviainen et al., 2015; Regenspurg et al., 2004). Considering the ability of schwertmannite to remove As and other potentially toxic species from solution (Carlson et al., 2003; Regenspurg and Peiffer, 2005), it is common in AMD environments to find schwertmannite enriched with these species in its structure. It has been proven that the presence of Cu(II) in the schwertmannite structure does not only decrease the transformation rate to goethite, but also increases its capacity for As retention by a factor of ~25% (Antelo et al., 2013). The sorption capacity of schwertmannite drastically decreases during the transformation towards more stable and crystalline forms (Antelo et al., 2013; Baleeiro et al., 2018; Burton and Johnston, 2012), which emphasizes the importance of preventing schwertmannite from ageing to naturally mitigate the mobility of trace metals and metal(loid)s in AMD or acidic landscapes. Burton et al. (2010) and Fan et al. (2019a) also reported a delay in the schwertmannite-goethite transformation under Fe(II)-rich reducing conditions in the presence of arsenate or chromate ions. Therefore, the presence of structural or adsorbed oxyanions produce an inhibitory effect on the transformation of schwertmannite towards more stable mineral phases (Regenspurg and Peiffer, 2005; Schoepfer et al., 2017).

The aim of the present study was to analyse the effect that the incorporation of arsenic and the presence of reducing agents such as Fe(II) or ascorbic acid have on the stability and adsorption behaviour of iron precipitates collected from an AMD affected area as well as on its synthetic analogue, schwertmannite. Arsenic and other metal(loid)s can be found associated with sulphide minerals and their oxidation products in mining environments. The formation of schwertmannite as a consequence of the sulphide minerals oxidation in AMD areas provides large surface areas and functional groups that allow the adsorption of pollutants, predominantly metals and metal(loid)s. We intend to contribute to a better understanding of the processes and factors that can prevent schwertmannite from ageing and thus pollutants from being remobilised into the soil solution or aqueous systems.

2. Materials and methods

2.1. Reagents

Arsenate was purchased as potassium monobasic salt from Sigma. Metal standard solutions of Sigma-Aldrich were used to calibrate the AAS and ICP-OES. All other chemicals were of

111 Merck p.a. quality. The experiments were carried out using double-distilled and CO_2 free
112 water, apart from the experiments conducted in reducing conditions where solutions were
113 prepared in pre-boiled double-distilled water, which was also purged with N_2 to avoid the
114 presence of CO_2. A-grade glassware and polycarbonate material were used in the preparation
115 of stock solutions, the synthesis and the adsorption and transformation experiments. All
116 glassware and polyethylene bottles were washed with 10% HNO_3 and rinsed with ultrapure
117 water to prevent contamination by metals. All chemical analysis were conducted at least by
118 duplicate to ensure the reproducibility of the results obtained.
119
120 **2.2. Field sites sampling and characterization**
121 Water and sediment samples were collected from a stream affected by AMD in the
122 mine of Touro (NW Spain) in October 2014. This mine was initially exploited in the early
123 70's for copper extraction from the main ore minerals chalcopyrite and pyrrhotite. After the
124 mine was closed in 1988 the area was confined to extraction of materials for road
125 construction. Periodical environmental monitoring analyses and different remediation efforts
126 have been conducted at the critical sites and in soils and water streams in the affected area.
127 Three water samples, *POR1*, *POR3* and *POR5*, were collected from Portapego stream,
128 which crosses through the mining area in Touro. Electrical conductivity (EC), pH, dissolved
129 oxygen, redox potential and temperature of the water samples were measured *in situ* using a
130 multi-parameter probe (Hach HQ 40d). These samples were filtered through 0.45 μm
131 Millipore filters in the field, and subsamples were acidified with 1% HNO_3 for subsequent
132 metal determination in the laboratory. Total Fe, Al, Cu, Zn, Ni and Mn were determined in the
133 water samples by Atomic Absorption Spectroscopy (AAS) (Perkin-Elmer PinAAcle 500),
134 while the concentration of Fe(II) was determined by the 1,10-phenanthroline method of
135 (Clesceri et al., 1998). The concentration of sulphate was measured by a turbidimetric method
136 (Clesceri et al., 1998) with a JASCO V-530 UV/Vis spectrophotometer.
137 The iron-rich AMD bed sediments were collected from the surface layer (0-10 cm) and
138 samples were transported in polyethylene flask at 4 ºC in darkness. Then samples were left to
139 dry at room temperature prior to granulometric separation through 0.5 mm and 63 μm sieves.
140 The smaller fraction was used for characterization. Microwave assisted acid digestion of the
141 AMD sediments (fraction < 63 μm) was conducted in order to determine their chemical
142 composition. A mixture of 37% HCl (3 mL) and 65% HNO_3 (9 mL) was added to 0.5 g of the
143 solid samples in Teflon containers protected with porcelain covers and placed in the digester
144 (Millestone Ethos Plus), where temperature can reach 200 °C. The solution obtained was

diluted to a final volume of 50 mL with milliQ water. The concentration of major and trace metals (Fe, Al, Cr, Cu, Ni, and Zn) was determined by Atomic Absorption Spectroscopy (AAS) (Perkin-Elmer PinAAcle 500) and the concentration of sulphate by the turbidimetric method previously used for water samples.

Poorly crystalline iron and aluminium amorphous and semi-crystalline oxides were extracted with ammonium oxalate following the procedure proposed by Mckeague and Day (1966). Briefly, 0.5 g of the samples were mixed with 50 mL of 0.2 M oxalic acid/ammonium oxalate (buffered at pH 3) in centrifuge tubes. During 4 h the tubes were left in an orbital shaker (Rotabit J.P. Selecta) in the dark to prevent the photoreduction of iron. After this time, the suspensions were centrifuged at 5000 rpm for 10 min (Orto Alresa Digitor) and the supernatants were filtered through 0.45 mm Millipore filters. Fe and Al concentrations in solution were determined by AAS. The concentration of sulphate was measured as previously indicated.

Powder X-ray diffraction (XRD) patterns (Phillips PW1710 diffractometer) of the sediments were obtained in order to identify the iron phases. Measurements were conducted between 15° and 65° 2θ, with a step size of 0.02° and counting time of 3 s per step.

2.3. Preparation and characterization of synthetic analogues

Schwertmannite (*Sch*) was prepared following a procedure similar to that proposed by Bigham et al. (1990). Briefly, $FeCl_3 \cdot 6H_2O$ (10.8 g) and Na_2SO_4 (3 g) were added to 2 L of distilled water preheated at 60 °C. The mixture was maintained at 60 °C for 12 min. After cooling at room temperature, the suspension was dialysed in double-distilled water for 33 days and finally freeze-dried (Telstar Cryodos LIOBETA-S0) to obtain the final powder. The sulphate and iron content of the synthetic sample were determined following digestion of the solid sample with 6 M HCl. Sulphate was determined as previously indicated whereas iron content was measured by ICP-OES (Perkin-Elmer Optima 3300DV). The solid phase was also characterized by XRD.

Jarosite (*Jar*) was synthesized following the procedure proposed by Baron and Palmer (1996). $Fe_2(SO_4)_3 \cdot nH_2O$ (17.2 g) and KOH (5.6 g) were dissolved in 100 mL of double-distilled water. The suspension was allowed to boil moderately during 4 hours under continuous stirring at approximately 96 °C. During this time, the colour of the suspension changed from reddish to yellow, indicating the formation of the desired phase. Then the solid precipitate was allowed to settle, discarding the supernatant. Finally, the precipitate was washed with distilled water to remove other ions on the surface and the solid was dried for 24

h at 110 °C and stored until use. The chemical composition of the sample was determined by ICP-OES following microwave assisted digestion with *aqua regia*. The jarosite crystalline phase was identified by XRD.

The goethite sample (*Gt*) had been synthesized by Otero-Fariña et al. (2017) following the method recommended by Cornell and Schwertmann (1996). Goethite characterization was also conducted in the same study.

2.4. Arsenic adsorption

Batch adsorption experiments were performed in order to determine the amount of arsenate adsorbed as a function of pH. The adsorption of arsenic was conducted on the synthetic analogues (*Sch*, *Jar*, *Gt*) and on the sediment sample *POR3*. Arsenate was added to the suspensions (1 g/L in 0.1 M KNO_3) at different As/Fe molar ratios (0.07, 0.12, 0.30 and 0.48). The pH was adjusted with 0.1 M HNO_3 and KOH standard solutions within the range 2 to 9. First adjustment was made immediately after the addition of the arsenic and once again 6-7 hours after the addition. The suspensions were shaken for 24 h (*Gt*, *Jar*) or 72 h (*Sch*, *POR3*), and then filtered through 0.45 μm Millipore filters and kept at 4 °C until analysis. Preliminary kinetic experiments showed that a contact time of 72 h was required to achieve equilibrium for *Sch* and *POR3*, while a shorter time was needed for *Gt* and *Jar*. The concentration of arsenate in solution was determined by the colorimetric method proposed by Lenoble et al. (2003) and the concentration of sulphate by a turbidimetric method (Clesceri et al., 1998). All the adsorption experiments were carried out in duplicate to ensure the reproducibility of the results obtained.

2.5. Transformation experiments

2.5.1. Ageing of the AMD sediments at constant pH

A long-term transformation experiment was carried out at pH 3 with a set of samples consisting of the raw sediments *POR1*, *POR3*, and *POR5* and synthetic schwertmannite, *Sch*, as a reference material. The transformation was also studied with these samples spiked with arsenate at As/Fe molar ratio 0.1. Samples in this set were labelled as *POR1As*, *POR3As*, *POR5As* and *SchAs*. Suspensions of 10 g/L of the AMD sediments and 1 g/L of *Sch* were prepared in double-distilled water and kept in 1 L polyethylene bottles at room temperature in an orbital shaker (HS 501 digital IKA Labortechnic) during the duration of the experiment. An aliquot of a stock arsenate solution was added to the suspension before completing the total volume of the suspension. The pH was then adjusted to 3 using small volumes of 1 M

NaOH or HNO_3. Another set of sub-samples using samples *POR3* were prepared to analyse the effect of pH (from 3 to 9) and As concentration (As/Fe from 0.64 to 3.22) in the ageing experiment. To better understand the experimental set up, all the information has been gathered in Table S1 (Supplementary Data). All the samples were placed on an orbital shaker and left to agitate at room temperature during 8 months. Following the first 24 hours of equilibration, a subsample of homogenized suspension was removed from the bottles, centrifuged, and filtered to determine the concentration of As, ensuring that most of the arsenate was sorbed on the mineral surface. Once a week, during the first two months, the pH was controlled and re-adjusted if necessary, after that, the control was made every two weeks. Temperature and electric conductivity were also checked periodically.

Suspension aliquots were withdrawn every 15 days during the first two months and once a month thereafter. The aliquots were then filtered through 0.45 μm Millipore filters and the concentrations of AsO_4 and SO_4 were measured by colorimetric (Lenoble et al., 2003) and turbidimetric (Clesceri et al., 1998) methods, respectively. At different time intervals, along with the supernatant, a fraction of the solid was also removed and analysed by XRD and XAS techniques. Aliquots of 100 mL were extracted and centrifuged at 6000 rpm during 10 min. The solid was washed three times and re-suspended with double-distilled water prior to freeze drying.

For samples *POR3*, *POR3As*, *Sch* and *SchAs* the Fe K-edge XAS spectra were collected, at ambient temperature and pressure, on beam line 7.3 at the Stanford Synchrotron Radiation Lightsource at SLAC National Laboratory Accelerator. Specifications of XAS measurements are the same as those detailed in previous studies (Kasiuliene et al., 2018). The line was equipped with a LN_2 cooled double-crystal Si (2 2 0) monochromator and rhodium-coated collimating mirror. The measurements were performed using an about 60% detuning to remove higher-order harmonic frequencies. XAS data were collected in transmission mode using ionization chambers as I0 and I1. The data was self-calibrated with a Fe foil placed between I1 and I2. Samples were finely grinded and the powder was evenly pasted on a Kapton tape. Subsequently, the Kapton tape was folded as many times as required to obtained about 90% absorption of the sample. Spectra were collected from –200 eV to +800 eV about the K-edge of Fe (7112 eV). The monochromator step size was 0.1 eV in the XANES region and 0.05 Å in the EXAFS region. The XAS spectra were the result of averaging three scans. XAS data calibration, normalization, averaging and lineal combination fitting with reference Fe–K EXAFS spectra for schwertmannite and goethite, were processed using ATHENA (Ravel and Newville, 2005).

2.5.2. Transformation experiments in the presence of Fe(II)

The stability of the AMD sample *POR3* has been also studied in anoxic conditions in the presence of Fe(II). Previous studies showed that the transformation rate of schwertmannite at pH > 5 is increased in the presence of Fe(II), although this process has been mainly studied in synthetic analogues rather than in natural samples (Burton et al., 2008; Burton et al., 2010; Fan et al., 2019a). A study of Burton et al. (2007) also attributed the relatively rapid transformation of natural schwertmannite on acidified coastal lowlands to the presence of Fe(II) ions. A 1 g/L suspension prepared in distilled water was introduced in a CRISON reaction cell, previously covered in aluminium foil, and bubbled with N_2 under constant stirring. The cell was hermetically closed in order to keep the conditions unaltered and through lid holes several probes and capillary tubes were fitted: a pH electrode (Crison Micro pH 2002), a redox potential electrode (Ingold Combination Redox Pt4805-S7/120), a capillary tube for the addition of reagents, the N_2 entrance and a capillary tube connected to a peristaltic pump (Thermo Scientific 72-310-300) for extraction of the sample of the supernatant. Experiments were conducted at pH values between 3.5 and 7 with a Fe(II) concentration of 10 mM. A blank was prepared at each of the working pH in order to analyse the amount of sulphate released in absence of Fe(II). pH values below 5 were adjusted with a previously decarbonized 1 M KOH solution whereas higher pH values, 6 and 7, were adjusted using sulfonic buffers, PIPES ($C_8H_{18}N_2O_6S_2$) and HEPES ($C_8H_{18}N_2O_4S$). The concentration of the buffers was 1 M and the pH was adjusted prior to Fe(II) addition. To prevent oxic conditions, N_2 was bubbled in all the solutions involved and in the distilled water used for their preparation, and all the system was kept hermetically closed.

The duration of the experiment was 24 h. During this period aliquots were periodically withdrawn using the peristaltic pump for Fe(II) and SO_4 analysis. These samples were acidified and filtered through 0.45 μm Millipore filters before analysis. After 24 h, the remaining suspension was frozen and stored before freeze-drying. The solid was analysed by XRD (Phillips PW1710 X-ray diffractometer) to assess any mineralogical change at the end of the experiment.

2.5.3. Transformation experiments in the presence of ascorbic acid

The effect that the presence of a reducing agent has on the transformation of schwertmannite was studied by adding ascorbic acid in the system. The reductive dissolution experiments were conducted with samples *POR3* and *Sch*. Eight reactors were set up at different initial conditions for the two iron oxide samples (Table S2, Supplementary Data). Each reactor contained 200 mL of 0.01 M $NaNO_3$ and 0.2 g of *Sch* or *POR3* sample

(concentration in reactor 1 g/L). Every sample was analysed in the presence and in the absence of arsenate at two different pH values, 3 and 5. An arsenic to iron molar ratio of 0.1 was studied when arsenate was present in the system. Arsenate was allowed to equilibrate with the mineral for 5 hours prior to the addition of 250 μM ascorbic acid. Concentrations of Fe(II) in solution were not detected for any of the reactors prior to addition of ascorbic acid. The reactors were maintained in the dark under a continuous N_2 gas purging into the reactor during the course of the experiment. The deionized water used to prepare the solutions was degassed and subsequently N_2 gas was purged through it overnight before the experiment. The pH value of the desired experiment was controlled overnight prior to the experiment and it was periodically checked in the reactors to ensure that it remained constant during the experiment.

The first aliquot was collected before the addition of ascorbic acid as a control. Fe(II) concentration was measured by taking aliquots after 10, 30, 60, 120 and 180 min after the addition of ascorbic acid. All aliquots were filtered in the absence of light and filtrates were collected in foiled glass vials. Samples were acidified with sulfuric acid in order to prevent oxidation from Fe(II) to Fe(III). Iron concentrations were determined spectrophotometrically by the 1,10-phenanthroline method (Clesceri et al., 1998).

3. Results and discussion

3.1 Analysis of the AMD water samples

The results obtained in the physico-chemical characterization of the collected water samples are shown in Table S3 (Supplementary Data). The water samples have acidic pH, which is caused by the oxidation process of pyrite or any other mineral sulphide present. Nordstrom (2011) indicated that this oxidation process is accelerated in mining areas at contact with air or due to the presence of iron-oxidizing bacteria. Redox potential, which in acid mine waters indicates the degree of oxidation of the mineral sulphides, was lower in *POR5* and increases downstream towards sample *POR1* (Figure S1, Supplementary Data). The conductivity was high compared to unaffected stream waters but still lower than values measured in other AMD areas, such as Riotinto (in Huelva, Spain) where conductivity can reach 3000-4500 μS/cm (Asta el al., 2010). The AMD waters analysed are rich in Fe(II) and SO_4 ions, with concentrations above 30 and 500 mg/L, respectively. These values, along with the concentrations for the other major elements, are comparable to those found in other AMD sites (Asta et al., 2010; Sanchez-España et al., 2005). Concentrations of trace elements were

higher than in unaffected surface waters, which are generally lower than 1 μg/L (Nordstrom, 2011). Sample *POR1* systematically shows lower values in all the measured parameters. This can be explained considering the location of the sampling site, which is about 3 to 4 km downstream and outside the mining boundaries (Figure S1, Supplementary Data). Precipitation of iron oxyhydroxysulphate minerals is favoured at the sites closer to the AMD source, while formation of iron mineral forms without sulphate is favoured downstream (Asta et al., 2010).

In order to establish whether the mine water samples fall within the stability range of schwertmannite, pOH, pSO_4 and pFe were calculated from the data measured and the activity coefficients were determined using the Davies equation. These data can be plotted in a pFe + 3pOH *vs* pSO_4 + 2pH diagram (Figure 1), in which the stability and solubility lines of schwertmannite and ferrihydrite were also defined (Supplementary Data). As expected from the extremely acidic pH of the water samples, all of them fall within or very close to the stability region of schwertmannite. An abiotic neutralization experiment was conducted with a subsample of *POR3* following the method proposed by Baleeiro et al. (2018). Initially this water sample was located in the stability region of schwertmannite, but with increasing pH the sample moves to the stability region of ferrihydrite, which becomes predominant at pH > 4 (Figure 1).

Figure 1.

3.2 Sediments characterization

3.2.1 XRD

Diffractograms for the sediment samples and the synthetic analogues are shown in Figure 2. XRD diffractograms of the synthetic samples of schwertmannite, goethite and jarosite were used as references in order to identify iron mineral phases in the natural mining sediments. Schwertmannite exhibits a poor crystalline pattern with only three broad bands at ~17º, 35º and 45º 2θ (Bigham et al., 1994). The diffractogram of goethite, on the other hand, present several well defined and narrow peaks located at ~21.4º, 33.4º, 34.9º, 36.8º, and 53.5º 2θ. The pattern of jarosite is also recognizable for presenting many peaks very well defined, especially those at ~17.5º, 28.7º, 29.1º, 45.8º and 49.8º 2θ (Baron and Palmer, 1996).

Figure 2.

From the XRD patterns for the three AMD sediments (Figure 2) it can be said that although *POR1* diffractogram contents most of the characteristic peaks of goethite, these are not as well defined as in the pure phase. Some jarosite peaks were also detected in this sample, confirming the presence of more crystalline phases. Sample *POR5* is more similar to schwertmannite, with broad bands at ~27º and ~35º, whereas sample *POR3* can be considered as an intermediate phase because some broad bands of schwertmannite are combined with incipient narrower peaks of goethite. In this sample, the band at ~35° seems to begin its transformation into the three peaks characteristic of goethite.

3.2.2 Chemical composition

The composition of the sediments was determined following acid digestion of the samples (Table S4, Supplementary Data). All the samples presented lower Fe contents than the synthetic schwertmannite. On the other hand, sulphate concentration in natural and synthetic samples is very similar and within the typical range reported for schwertmannite (Caraballo et al., 2013). Only sample *POR1* has a sulphate concentration below this range. This fact is in agreement with the XRD results for this sample (Figure 2), where more and better defined peaks, similar to the goethite diffractogram pattern, can be observed. The Fe/S and Fe/Al molar ratios can be also analysed. These values once more serve to confirm the differences in the composition of sample *POR1* in comparison with the other two AMD samples.

Fe and Al concentrations extracted with oxalate (Table S4, Supplementary Data) allows for determining the percentage of Fe and Al associated to amorphous or low-crystallinity phases within the sediments. These results showed that 37.2%, 75.3% and 65.1% of total Fe in *POR1*, *POR3* and *POR5*, respectively, was present as an amorphous phase. In the case of Al, these percentages were 2.13%, 7.32% and 4.47% in *POR1*, *POR3* and *POR5*, respectively. These results confirm the presence of high amounts of iron amorphous oxides, that is, the low crystallinity of the sediments. Moreover, the concentration of amorphous phases are higher in the sediments collected upstream, closer to the AMD source, compared with those collected downstream. This is in agreement with the XRD results observed, since goethite-like particles were detected in sample *POR1*.

3.3 Arsenic adsorption

The results of batch adsorption experiments of arsenate on synthetic analogues and *POR3* sample using different As/Fe ratios are shown in Figure 3 and Figure S2

(Supplementary Data). Results indicate that the sorption of arsenate on the sediment is comparable to that on the synthetic *Sch* within the whole pH interval. This behaviour is supported by the XRD results (Figures 2), which showed that *POR3* sample was predominantly formed by schwertmannite. The arsenate sorption affinity of the synthetic samples and *POR3* sediment follows the sequence: *POR3* ~ *Sch* > *Gt* > *Jar*. At the lower As/Fe ratio (0.07), the amorphous phases, *Sch* and *POR3*, retained all the arsenate added whereas the sorption level decreased by 60% to 90% on the more crystalline phases *Gt* and *Jar*, respectively. At the higher As/Fe ratio (0.48), about 40% of the arsenate remained sorbed on *POR3* and *Sch*, whereas only 20% on *Gt* and less than 10% on *Jar*. These results are also in agreement with the crystallinity degree of the samples, since schwertmannite particles showed higher amorphous character and larger specific surface area values than *Gt* and *Jar*, respectively (Cornell and Schwertmann, 1996; Meng et al., 2020). Attending to these results, the transformation process from schwertmannite to goethite or other crystalline phases would increase the mobility of arsenate or other anionic species, e.g. chromate, phosphate or selenate. Thus, it is important to increase the stability of schwermannite minerals in AMD systems to extend their scavenging properties for contaminants.

Arsenate adsorption on samples POR3 and Sch can be compared with the results found in the literature for other schwertmannite samples. At low As/Fe ratios, < 0.15, and acidic pH values, adsorption levels are close to 100% (Burton et al., 2009; Fukushi et al., 2003), similarly to our findings. On the other hand, results obtained by Burton et al. (2009) at high As/Fe showed slightly higher adsorption levels, i.e. at pH 4 and As/Fe = 0.38, almost 80% of the As was adsorbed, while in the present study, at pH 4 and As/Fe = 0.30, around 75% of the As was adsorbed on both POR3 and Sch samples (Figure S2, Supplementary Data). The observed differences may be attributed to differences in the surface area or in the sulphate content. The effect of pH was not very pronounced and a slight decrease in adsorption at pH > 7 can only be observed at relatively high As loadings where sorption capacities were below 100%. Similarly, results found by Burton et al. (2009) also showed a slight decrease on the As adsorption level on schwertmannite after increasing the pH at relatively high As loading. Previous experiments with 2-line ferrihydrite showed a greater pH effect on the arsenate adsorption, i.e. the adsorption level dropped from 100% to 50% as the pH increased from 5.5 to 10 (Antelo et al., 2015). The adsorption decrease with the pH is caused by changes in the surface charge of the iron mineral oxides and in the concentration of sulphate groups present in the schwertmannite structure. Arsenate adsorption mechanism on iron oxides usually involves ligand exchange reactions with the iron hydroxyl groups at the

mineral surface, while in the case of schwertmannite anion exchange reactions with the sulphate groups present in the crystalline structure are also relevant.

Figure 3.

3.4. Transformation experiment of AMD sediments

3.4.1. Effect of arsenic on the ageing under oxic conditions

Ageing of the AMD sediment samples was evaluated over a period of 8 months at constant pH in the absence and in the presence of arsenate ions. The concentration of SO_4 measured in the solution over time at pH 3 (Figure 4) achieved a constant value during the ageing period in the presence of As in the mineral surface. This plateau was reached in between 60 and 120 days. Initially, the SO_4 concentration in solution was higher in the presence of As. This result can be explained by the mechanism of adsorption of arsenate onto schwertmannite. Arsenate adsorbs partially through an ion exchange reaction with sulphate within the first 48 to 72 hours of the reaction (Antelo et al., 2012; Burton et al., 2009). At longer times, 120 and 280 days, the samples in the absence of As showed a continuous increase of sulphate concentration in solution. This is in agreement with the results found by Bigham et al. (1996), showing an increase in the sulphate concentration released to the solution with the ageing time until a constant value was reached after 500 days. The results from Bigham et al. (1996) reflected a gradual transformation from schwertmannite to goethite through a hydrolysis reaction. The sulphate released in the absence of arsenate was plausibly due to mineral transformation processes whereas a great percentage of the sulphate released in the presence of arsenate is due to an anion exchange reaction. As stated above, anion exchange reactions involving structural sulphate ions is a relevant process for the immobilization of oxyanions on schwertmannite (Burton et al., 2009; Fukushi et al., 2003). Regenspurg and Peiffer (2005) reported the partial transformation of synthetic schwertmannite into goethite after one year, whereas no transformation was observed for Cr- and As-doped schwertmannite. The release of sulphate observed in these experiments thus suggested that the transformation of schwertmannite into goethite was slowed down by the presence of As. This indirect evidence will be, later in this subsection, supported by XRD and EXAFS data. Finally, for samples aged in the presence of As we observed a decrease in the SO_4 concentration in solution after 150 days, which could be related to a re-adsorption process on the mineral surface. The variation of the concentration of As in solution during the ageing experiment was also measured and results are shown in Figure S3 (Supplementary

Data). Results showed that after 24 hours the uptake of the As is higher than 90%, with sample *POR1As* showing the lowest As uptake. This is in agreement with the results for the sulphate release in the presence of As (Figure 4), since this sample showed the lowest sulphate concentration in solution. Throughout the ageing experiment no release of As was observed in these samples, being the % of As released lower than 1% after 60 days. This also supports the slower transformation rate when As is present, since the change to more crystalline phases should promote the release of adsorbed ions and higher concentrations in solution should be observed.

Figure 4.

Ageing experiments were also conducted with sample *POR3* at variable As concentrations at pH 3, 7 and 9 (Figures S4 and S5, Supplementary Data). At pH 3 and pH 7, as the concentration of As increases, more sulphate is released from the AMD samples. This fact can be explained by the anion exchange between the arsenate added and the structural sulphate present in solid (Antelo et al., 2012; Burton et al., 2009; Fukushi et al., 2007). At pH 9 sulphate concentration was similar in both the absence and the presence of As. This is due to the high concentration of hydroxyl ions in the system, which favours the release of structural sulphate through ion exchange (Boily et al., 2010), combined with the lower affinity of schwertmannite for As at pH 9 (Antelo et al., 2012). Regardless of the As/Fe ratio, at pH 3 and 7, less than 0.5 % of the initial As concentration was measured in solution during these ageing experiments. Only at pH 9, and at the highest As/Fe ratio, a significant concentration of As was detected in solution, between 20.8% and 1.6% of the initial As at 24 h and 57 days, respectively (Figure S5, Supplementary Data). These results are in agreement with previous findings showing that an increase of pH increases the transformation rate of schwertmannite to goethite, especially at pH above 7 (Regenspurg et al., 2004; Jönsson et al., 2005).

The XRD patterns for natural AMD sediments and synthetic schwertmannite were collected at different times (Figure 5 and Figure S4, Supplementary Data). The diffractograms confirmed the indirect evidences indicated by sulphate release to the solution. After 91 days, the diffractogram for *Sch* started to show diffraction peaks at ~22°, ~35° and in the region between 50° and 65°. These diffraction peaks were assigned to the formation of goethite. The diffractogram of the sample spiked with As remained similar to that of *Sch* at the initial stage. After 150 days, in the absence of As, the diffraction peaks stemming from goethite became

sharper and more intense whereas in the presence of As some initial peaks of goethite started to be detected at ~22° and ~53°. Thus, the presence of As, either adsorbed on the mineral surface or incorporated in the crystalline structure substituting sulphate groups, retarded the mineral transformation process from schwertmannite to goethite. The XRD data collected for *POR3* showed similar behaviour than synthetic schwertmannite. Diffractograms for samples *POR1* and *POR5* collected at 91 days are shown in Figure S6 (Supplementary Data). *POR1* was originally more similar to goethite since the collection point was further away from the mine and both pH and sulphate concentration made it less favourable for schwertmannite formation at these conditions (Figure 1). Since goethite was initially detected in *POR1*, diffractograms after ageing, with and without As, do not show significative differences compared with the original sample. XRD data of ageing experiments of sample collected at *POR5* showed a similar behaviour to *POR3, i.e*. the presence of arsenic delayed the transformation of schwertmannite into goethite.

Figure 5.

XRD data was in good agreement with Fe k-edge EXAFS recorded on the same samples (only at *POR3*) (Figures 6 and 7). Figure 6 shows the evolution of the EXAFS spectra for the samples *Sch* and *POR3*, in the absence and in the presence of As, during the ageing experiment. These spectra were well described by linear combination fitting (LCF) calculations over the k-range 3 to 13 $Å^{-1}$ using schwertmannite and goethite as standard spectra. The fitting parameters for the aged samples are shown in Table S5 (Supplementary Data). The spectra of *Sch* and *Gt* displayed distinctive features at k ~5 $Å^{-1}$, and differences at higher k values, above 8 $Å^{-1}$, allowing the distinction between both phases in the transformed samples.

Figure 6.

Figure 7 shows the fraction of goethite, as obtained by LCF of the spectra shown in Figure 6, present at different ageing times both for *Sch*, and for AMD sediments at *POR3*. The ageing experiments were performed in suspensions at pH 3 and in the presence or in the absence of As in the system. On one hand, in the absence of arsenate (triangles and rhomboids) the transformation of schwertmannite into goethite was observed, with a final content of goethite between 40 and 60%. *Sch* transformed to a slightly higher degree than the schwertmannite

present in the sediment *POR3* did. The amount of goethite found in the *Sch* was found to be about 20 % higher in the range of time studied. Changes in the initial degree of crystallinity between *Sch* and the AMD sediments or slight incorporation/adsorption of other elements, such as Al or Cu in sediments, could explain the change in the transformation rate between the two samples. The incorporation of Cu or other trace elements on the mineral structure or mineral surface has been previously reported to increase the stability of schwertmannite (Antelo et al., 2013; Fan et al., 2019b). On the other hand, the arsenic bearing samples did not undergo a great extent of transformation into goethite in the range of time studied. Only a slight transformation into goethite, about 10%, was observed in *SchAs* after 276 days of experiment whereas no transformation at all could be detected in the sediment *POR3As*. Again, *SchAs* showed to have a higher transformation rate towards goethite than the As doped sediment as observed in the experiments without arsenate in the system.

Figure 7.

3.4.2 Transformation experiment in the presence of Fe(II)

The aim of this experiment was to assess the role of Fe(II) ions in the mineralogical transformation of natural iron oxy(hydroxy)sulphates. Changes in the solid phase and in the solution were monitored by collecting XRD diffractograms and by measuring the concentration of SO_4 and Fe(II) during a 24 h period. The sulphate release to the solution was pH dependent (Figure 8), with the highest concentrations found at pH 6 and 7. Similar trends have been reported for schwertmannite by several authors (Antelo et al., 2013; Burton et al., 2009; Paikaray et al. 2017; Regenspurg et al., 2004), although longer times were required in the absence of Fe(II) to achieve the same levels of sulphate release. It can be observed that at pH 6 and 7, there is a significant increase in the concentration of sulphate due to the presence of Fe(II) ions (Figure 8), specially at longer experimental times, *i.e*. above 15 hours. After 24 h, the SO_4 in solution at pH 6 comprises approximately 60% of the total sulphate in the solid phase whereas it reaches almost 100% (179 mg/L) at pH 7. At pH < 6, however, Fe(II) showed no significant effect on the SO_4 release. The variation in the concentration of Fe(II) and the redox potential of the solution during the transformation experiment can be observed in Figure 9. Fe(II) concentration decreased faster at pH 6 than it did at pH 7, inversely to the SO_4 concentration released. The redox potential, on the other hand, increases as the Fe(II) disappears from solution. This variation is faster at pH 7 than at pH 6. However, after 15-20 h practically all the Fe(II) in the system was consumed. This can be explained by the high

affinity of this ion for the surface of iron (oxy)hydroxides at pH > 5 (Burton et al., 2008; Hinkle et al., 2015). Following adsorption on the mineral surface, Fe(II) ions catalyse the transformation of amorphous iron oxides to more crystalline phases through an Ostwald ripening process. The Fe(II) electron transfer to the structural Fe(III) enhances the reductive dissolution rate and favours the consequent re-precipitation as a more stable mineral phase. This mechanism was proposed by Hansel et al. (2005), who observed that the evolution of ferrihydrite to goethite (or lepidocrocite) is accelerated as the Fe(II) concentration in solution increases. From this experiments it can be concluded that the presence of Fe(II) ions in anoxic environments has a key role as a catalyser in the transformation of the iron oxy(hydroxy)sulphates present in areas affected by AMD. These results confirm the previous findings of Burton et al. (2007), which showed that the interaction between Fe(II) ions and natural schwertmannite in reducing conditions promotes the formation of goethite in acid-sulphate soils.

XRD patterns of the solid samples collected at the end of the experiment (Figure 8) are in agreement with the changes observed in the solution. At pH 4 and 5, schwertmannite is the only mineral phase detected in the diffractogram, while more crystalline phases were observed at higher pH values. XRD data at pH 7 showed that the dominant phase was goethite. At pH 6, goethite peaks were also observed, although the most intense peaks were observed at ~18 º and ~22º. These peaks were assigned to the presence of roemerite, a hydrated iron sulphate mineral containing both Fe(II) and Fe(III) in their structure ($Fe^{2+}Fe^{3+}_2(SO_4)_4 \cdot 14H_2O$). Finally, to assess if the co-presence of arsenic has any effect on the Fe(II)-catalyzed transformation of schwertmannite, additional experiments were conducted at pH 6 and 7 with both Fe(II) and As present in the system. The XRD of the samples collected after 24 h showed that schwertmannite is the dominant phase at pH 6 (Figure S7, Supplementary Data), pointing out the stabilizing effect of the arsenic. This is in agreement with previous results obtained by Fan et al. (2019a) and Schoepfer et al. (2019). Both studies indicate that the presence of As or P decrease the Fe(II)-induced transformation of schwertmannite at pH 6.5. As stated above, in order to have the electron transfer reactions that promote the formation of goethite, Fe(II) ions need to be initially adsorbed on the schwertmannite surface. However, when As is present in the system both ions may compete for the same binding sites at the mineral surface. Increasing the pH from 6 to 7 lead to the formation of goethite peaks, although the intensity of these peaks is slightly lower than the observed in the absence of As (Figure S7, Supplementary Data). It should be kept in mind that

583 increasing the pH favours the adsorption of Fe(II) ions on iron oxides, while arsenate
584 adsorption may decrease (Antelo et al., 2015; Hinkle et al., 2015).
585
586 **Figure 8**.
587
588 **Figure 9**.
589
590 **3.4.3 Effect of arsenic on the reductive dissolution by ascorbic acid**
591 The reductive dissolution of synthetic schwertmannite and sediment samples from
592 *POR3*, using ascorbic acid as a reductant, was studied in the presence and in the absence of
593 arsenic. The ascorbic acid acts as an electron donor which reduces Fe(III) into Fe(II) (Dos
594 Santos Afonso et al., 1990). As a consequence Fe(II) releases into solution. It was assumed
595 that at the low pH conditions at which the experiments were performed the extent of the
596 further transformation of schwertmannite due to the presence of Fe(II) in the system was
597 insignificant and only the reductive dissolution was assumed to take place to a significant
598 extent. The latter assumption was based on the low degree of adsorption of Fe(II) ions on iron
599 oxides at those pH values (Hinkle et al., 2015; Hiemstra and van Riemsdijk, 2007), as well as
600 the low level of re-adsorption in the presence of ascorbate in the system (Deng et al., 1997).
601 Figure 10 shows the concentration of dissolved Fe(II) as function of the time from which
602 ascorbic acid was added to the schwertmannite suspensions. The concentration of Fe(II) was
603 undetectable prior to addition of ascorbic acid to the system. The left figure shows data
604 describing the reductive dissolution of *Sch* at pH 3 and at pH 5 whereas the figure on the right
605 shows data describing the reductive dissolution of sediments collected at *POR3*. The presence
606 of arsenic in the system did not significantly change the kinetics of reduction of iron of any of
607 the two samples at any pH value. A decrease of Fe(II) in solution could have been anticipated
608 since arsenic changed the transformation rate of schwertmannite in aerobic conditions.
609 However, no change in schwertmannite reactivity was observed under these reductive
610 conditions. These findings are supported by the results published by Pedersen et al. (2006),
611 where it was shown that the rate of reduction of other iron oxides, such as ferrihydrite,
612 goethite and lepidocrocite, was also unaffected by the presence of arsenic when using
613 ascorbic acid as a reducing agent. Interestingly, the amount of Fe(II) dissolved from the
614 sediments was lower than the amount dissolved from the synthetic schwertmannite. This
615 could be explained by the fact that the total content of Fe in *Sch* was higher than the total
616 amount of iron found in sediments at *POR3*, 8.88 mmol/g and 6.45 mmol/g, respectively as

described earlier in Table S4 (Supplementary Data). However, when normalizing by the amount of iron in the sample, the amount of dissolved Fe(II) was consistently 60 % higher for synthetic schwertmannite than for sediments. Several factors could explain this behaviour. Among others, one factor could be that *Sch* showed different crystallinity levels compared with the AMD sediments. Another factor could be the incorporation/adsorption of other elements such as Al or Cu. This could change the reactivity of schwertmannite minerals (e.g. Antelo et al. 2013; Gan et al., 2015; Regenspurg and Peiffer, 2005). *Sch* and *POR3* showed higher degree of reductive dissolution at pH 3 than at pH 5, which is in agreement with previous literature results (Dos Santos Afonso et al. 1990; Cornell and Schwertmann, 1996).

Figure 10.

4. Conclusions

Schwertmannite-rich mine sediments showed high adsorption capacities towards arsenate. Unlike the adsorption of arsenate on other iron oxide minerals such as ferrihydrite, the adsorption on schwertmannite was less dependent on pH. The secondary precipitation of iron oxides, such as schwertmannite, has thus a high potential as a self-managed immobilisation of metal(loid)s in AMD. For an immobilisation method to be successful it needs to remain effective in time. Adsorption data showed that further crystallization of schwertmannite would lead to a possible remobilization of arsenate.

The combination of wet experiments, X-ray diffraction and XAS demonstrated that arsenate significantly delayed the transformation of schwertmannite into goethite. Preventing the crystallization of amorphous iron secondary minerals favours the long-term immobilization of trace elements under oxic conditions. Sensitive factors that would define the long-term self-managed immobilisation in AMD systems would be the pH and redox potential. Experiments conducted in the presence of Fe(II) ions and organic reducing agents promote the reductive dissolution of schwertmannite, which may have implications in the remobilization of arsenic and other metal(loid)s present on the mineral surfaces. The presence of arsenic in the system inhibited the Fe(II)-catalyzed transformation of schwertmannite, while it did not affect the rate of reductive dissolution caused by the ascorbic acid. Increasing the knowledge of the biogeochemical processes controlling the stability and reactivity of AMD minerals is a crucial tool for the management of mining sites, with the objective of either immobilizing contaminants or recovering critical raw materials.

Acknowledgements

S.F. and J.A. belong to the CRETUS-Institute (ED431E_2018/01), co-funded by FEDER (UE) and were also supported by the Group of Excellence GI-1245 financed by the Xunta de Galicia (Consolidation of competitive groups of investigation; GRC GI 1574). Åforsk and Wallenberg Foundation is acknowledged for financial support to I.C. Stanford Synchrotron Radiation Lightsource is acknowledged for granting our beamtime proposal (4663) under which X-Ray absorption measurements presented in this work were performed. Authors would like to thank the use of RIAIDT-USC analytical facilities.

REFERENCES

Antelo, J., Fiol, S., Gondar, D., López, R., Arce, F., 2012. Comparison of arsenate, chromate and molybdate binding on schwertmannite: surface adsorption vs anion-exchange. Journal of Colloid and Interface Science 386, 338-343.

Antelo, J., Fiol, S., Gondar, D., Pérez, C., López, R., Arce, F., 2013. Cu(II) incorporation to schwertmannite: Effect on stability and reactivity under AMD conditions. Geochimica et Cosmochimica Acta 119, 149-163.

Antelo, J., Arce, F., Fiol, S., 2015. Arsenate and phosphate adsorption on ferrihydrite nanoparticles. Synergetic interaction with calcium ions. Chemical Geology 410, 53–62.

Arán, D., Antelo, J., Fiol, Macías, F., 2018. Immobilization of phosphate by a Technosol spolic silandic: kinetics, equilibrium and dependency on environmental variables. Journal of Soils and Sediments 18, 2914-2923.

Asta, M.P., Ayora, C., Román-Ros, G., Cama, J., Acero, P., Gault, A.G., Charnock, J.M., Bardelli, F., 2010. Natural attenuation of arsenic in the Tinto Santa Rosa acid stream (Iberian Pyritic Belt, SW Spain): The role of iron precipitates. Chemical Geology 271, 1-12.

Baleeiro, A., Fiol, S., Otero-Fariña, A., Antelo, J., 2018. Surface chemistry of iron oxides formed by neutralization of acidic mine waters: removal of trace metals. Applied Geochemistry 89 129-137.

Baron, D., Palmer, C.D., 1996. Solubility of jarosite at 4-35 °C. Geochimica et Cosmochimica Acta 60, 185-195.

683 Bigham, J.M., Schwertmann, U., Carlson, L., Murad, E., 1990. A poorly crystallized
684 oxyhydoxysulfate of iron formed by bacterial oxidation of Fe(II) in acid mine waters.
685 Geochimica et Cosmochimica Acta 54, 2743–2758.
686 Bigham, J.M., Carlson, L., Murad, E., 1994. Schwertmannite, a new iron oxyhydroxysulphate
687 from Pyhäsalmi, Finland, and other localities. Mineralogical Magazine 58, 641-648.
688 Bigham, J.M., Schwertmann, U., Traina, S.J., Winland, R.L., Wolf, M., 1996.
689 Schwertmannite and the chemical modeling of iron in acid sulfate waters. Geochimica
690 et Cosmochimica Acta 60, 2111-2121.
691 Bigham, J.M., Nordstrom. D.K., 2000. Iron and aluminium hydroxysulfates from acid
692 sulphate waters, in: Alpers, C.N., Jambor, J.L., D.K. Nordstrom, D.K. (Eds,), Reviews
693 in Mineralogy and Geochemistry – Sulfate Minerals: Crystallography, Geochemistry,
694 and Environmental Significance, The Mineralogical Society of America, Washington,
695 DC, pp. 351-403.
696 Boily, J.F., Gassman, P.L., Perethyazhko, T., Szayi, J., Zachara, J.M., 2010. FTIR spectral
697 components of schwertmannite. Environmental Science & Technology 44, 1185-1190.
698 Burton, E.D., Bush, R.T., Sullivan, L.A., Mitchell, D.R.G., 2007. Reductive transformation of
699 iron and sulfur in schwertmannite-rich accumulations associated with acidified coastal
700 lowlands. Geochimica et Cosmochimica Acta 71, 4456-4473
701 Burton, E.D., Bush, R.T., Sullivan, L.A., Mitchelk, D.R.G., 2008. Schwertmannite
702 transformation to goethite via the Fe(II) pathway: Reaction rates and implications for
703 iron–sulfide formation. Geochimica et Cosmochimica Acta 72, 4551-4564.
704 Burton, E.D., Bush, R.T., Johnston, S.G., Watling, K.M., Hocking, R.K., Sullivan, L.A.,
705 Parker, G.K., 2009. Sorption of arsenic(V) and arsenic(III) to schwertmannite.
706 Environmental Science & Technology 43, 9202-9207.
707 Burton, E.D., Johnston, S.G., Watling, K., Bush, R.T., Keene, A.F., Sullivan, L.A., 2010.
708 Arsenic effects and behaviour in association with the Fe(II)-catalyzed transformation
709 of schwertmannite. Environmental Science & Technology 44, 2016-2021.
710 Burton, E.D., Johnston, S.G., 2012. Impact of silica on the reductive transformation of
711 schwertmannite and the mobilization of arsenic. Geochimica et Cosmochimica Acta
712 96, 134-153.
713 Caraballo, M.A., Rimstidt, J.D., Macías, F., Nieto, J.M., Hochella Jr., M.F., 2013.
714 Metastability, nanocrystallinity and pseudo-solid solution effects on the under-
715 standing of schwertmannite solubility. Chemical Geology 360-361, 22-31.

716 Carlson, L., Bigham, J.M., Schwertmann, U., Kyek, A., Wagner, F., 2003. Scavenging of As
717 from acid mine drainage by schwertmannite and ferrihydrite: A comparison with
718 synthetic analogues. Environmental Science & Technology 36, 1712-1719.
719 Clesceri, L.S., Greenberg, A.E., Eaton, A.D., 1998. Standard Methods for the Examination of
720 Water and Wastewater. American Public Health Association, Washington DC.
721 Cornell, R.M., Schwertmann U., 1996. The Iron Oxides: Structure, Properties, Reactions,
722 Occurrence and Uses. VCH Publishers, New York.
723 Deng, Y., 1997. Effect of pH on the reductive dissolution rates of iron(III) hydroxide by
724 ascorbate. Langmuir, 13, 1835-1839.
725 Dos Santos Afonso, M., Morando, P.J, Blesa, M.A., Banwart, S., Stumm, W., 1990. The
726 reductive dissolution of iron oxides by ascorbate. The role of carboxylate anions in
727 accelerating reductive dissolution. Journal of Colloid and Interface Science 138, 74-
728 82.
729 Fan, C., Guo, C., Zeng, Y., Tu, Z., Ji. Y. Reinfelder, J.R., Chen, M., Huang, W., Lu., G., Yi,
730 X., Dang, Z., 2019a. The behavior of chromium and arsenic associated with redox
731 transformation of schwertmannite in AMD environment. Chemosphere 222, 945-953.
732 Fan, C., Guo, C., Chen, M., Huang, W., Wan, J., Reinfelder, J.R., Li, X., Zeng, Y., Lu, G.,
733 Dang, Z., 2019b. Transformation of cadmium-associated schwertmannite and
734 subsequent element repartitioning behaviors. Environmental Science and Pollution
735 Research 26, 617-627.
736 Fukushi, K., Sato, T., Yanase, N., 2003. Solid-solution reactions in As(V) sorption by
737 schwertmannite. Environmental Science & Technology 37, 3581-3586.
738 Gan, M., Sun, S., Zheng, Z., Tang, H., Sheng, J., Zhu, J., Liu, X., 2015. Adsorption of Cr(VI)
739 and Cu(II) by $AlPO_4$ modified biosynthetic Schwertmannite. Applied Surface Science
740 356, 986-997.
741 Hansel, C.M., Benner, S.G., Fendorf, S., 2005. Competing Fe(II)-induced mineralization
742 pathways of ferrihydrite. Environmental Science & Technology 39, 7147-7150.
743 Hiemstra, T., van Riemsdijk, W.H., 2007. Adsorption and surface oxidation of Fe(II) on metal
744 (hydr)oxides. Geochimica et Cosmochimica Acta, 71, 5913-5933
745 Hinkle, M.A.G., Wang, Z., Giammar, D.E., Catalano, J.G., 2015. Interaction of Fe(II) with
746 phosphate and sulfate on iron oxide surfaces. Geochimica et Cosmochimica Acta 158,
747 130-146.

748 Jönsson, J., Persson, P., Sjöberg, S., Lövgren, L., 2005. Schwertmannite precipitated from
749 acid mine drainage: phase transformation, sulphate release and surface properties.
750 Applied Geochemistry 20, 179-191.
751 Jönsson, J., Sjöberg, S., Lövgren, L., 2006. Precipitation of secondary Fe(III) minerals from
752 acid mine drainage. Applied Geochemistry 21, 437-445.
753 Karimian, N., Johnston, S.G., Burton, E.D., 2018. Iron and sulfur cycling in acid sulfate soil
754 wetlands under dynamic redox conditions: A review. Chemosphere 197, 803-816.
755 Kasiuliene, A., Carabante, I., Bhattacharya, P., Caporale, A.G., Adamo, P., Kumpiene, J.,
756 2018. Removal of metal(oid)s from contaminated water using iron-coated peat
757 sorbent. Chemosphere 198, 290-296.
758 Kumpulainen, S., Räsänen, M.L., von der Kammer F., Hofmann, T., 2008. Ageing of
759 synthetic and natural schwertmannites at pH 2–8. Clay Minerals 43, 437–448.
760 Lenoble, V., Deluchant, V., Serpaud, B., Bollinger, J.C., 2003. Arsenite oxidation and
761 arsenate determination by the molybdene blue method. Talanta 61, 267-276.
762 Lozano, A., Ayora, C., Fernández-Martínez, A., 2019. Sorption of rare earth elements onto
763 basaluminite: The role of sulfate and pH. Geochimica et Cosmochimica Acta 258, 50-
764 62.
765 Lozano, A., Ayora, C., Fernández-Martínez, A., 2020. Sorption of rare earth elements on
766 schwertmannite and their mobility in acid mine drainage treatments. Applied
767 Geochemistry 113, 104499.
768 McKeague, J.A., Day, J.H., 1966. Dithionite- and oxalate-extractable Fe and Al as aids in
769 differenciating various classes of soils. Canadian Journal of Soil Science 46, 13-22.
770 Meng, X., Zhang, C., Zhuang, J., Zheng, G., Zhou, L., 2020. Assessment of schwertmannite,
771 jarosite and goethite as adsorbents for efficient adsorption of phenanthrene in water
772 and the regeneration of spent adsorbents by heterogeneous fenton-like reaction.
773 Chemosphere 244, 125523.
774 Moodley, I., Sheridan, C.M., Kappelmeyer, U., Ackil, A., 2018. Environmentally sustainable
775 acid mine drainage remediation: Research developments with a focus on waste/by-
776 products. Minerals Engineering 126, 207-220.
777 Nordstrom, D.K., 2011. Mine waters: Acid to circumneutral. Elements 7, 393–398.
778 Nordstrom, D.K., Alpers, C.N., 1999. Geochemistry of acid mine waters, in: The
779 Environmental Geochemistry of Mineral Deposits, Plumlee, G.S., Logsdon, M. (Eds.),
780 Society of Economic Geologists, pp. 133-160.

781 Otero-Fariña, A., Fiol, S., Arce, F., Antelo, J., 2017. Effects of natural organic matter on the
782 binding of arsenate and copper onto goethite. Chemical Geology 459, 119-128.
783 Paikaray, S., Schröder, C., Peiffer, S., 2017. Schwertmannite stability in anoxic Fe(II)-rich
784 aqueous solution. Geochimica et Cosmochimica Acta 217, 292-305.
785 Parviainen A., Cruz-Hernández, P., Pérez-López, R., Nieto, J.M., Delgado-López, J.M., 2015.
786 Raman identification of Fe precipitates and evaluation of As fate during phase
787 transformation in Tinto and Odiel River Basins. Chemical Geology 398, 22-31.
788 Pedersen, H.D., Postma, D., Jakobsen, R., 2006. Release of arsenic associated with the
789 reduction and transformation of iron oxides. Geochimica et Cosmochimica Acta 70,
790 4116-4129
791 Ravel, B., Newville, M. (2005). ATHENA, ARTEMIS, HEPHAESTUS: data analysis for X-
792 ray absorption spectroscopy using IFEFFIT. Journal of Synchrotron Radiation 12,
793 537-541.
794 Regenspurg, S., Brand, A., Peiffer, S., 2004. Formation and stability of schwertmannite in
795 acidic mining lakes. Geochimica et Cosmochimica Acta 68, 1185-119.
796 Regenspurg, S., Peiffer, S., 2005. Arsente and chromate incorporation in schwertmannite.
797 Applied Geochemistry 20, 1226-1239.
798 Sánchez-España, J., López-Pamo, E., Santofimia, E., Aduvire, O., Reyes, J., Barettino, D.,
799 2005. Acid mine drainage in the Iberian Pyrite Belt (Odiel river watershed, Huelva,
800 SW Spain): Geochemistry, mineralogy and environmental implications. Applied
801 Geochemistry 20, 1320-1256.
802 Schoepfer, V.A., Burton, E.D., Johnston, S.G., Kraal, P., 2017. Phosphate-imposed
803 constraints on schwertmannite stability under reducing conditions. Environmental
804 Science & Technology 51, 9739-9746.
805 Schoepfer, V.A., Burton, E.D., Johnston, S.G., 2019. Contrasting effects of phosphate on the
806 rapid transformation of schwertmannite to Fe(III) (oxy)hydroxides at near-neutral pH.
807 Geoderma, 340, 116-123.
808

Figure Captions

Figure 1. Plot of pFe + 3pOH *vs* pSO_4 + 2pH diagram for the mine water samples analysed. The closed circles correspond to the AMD water samples, and the open triangles correspond to the results of the abiotic neutralization experiment conducted with sample POR3 (here the arrow represents the increase of pH). The vertical dashed line represents the range of the stability boundary between schwertmannite and ferrihydrite of the waters in contact with both schwertmannite and ferrihydrite. The solid lines indicate the solubility of schwertmannite and ferrihydrite minerals.

Figure 2. X-ray diffractograms for the AMD sediments and the synthetic iron oxides. G – goethite; J – jarosite; S - schwertmannite

Figure 3. Arsenic adsorption as a function of pH and As/Fe molar ratio on *POR3* sediment sample (diamond) and synthetic iron oxides *Sch* (triangles), *Gt* (circles) and *Jar* (squares). (As/Fe molar ratios of 0.07 and 0.30 are shown in Figure S2, Supplementary Data).

Figure 4. Sulphate concentration released to the solution by the AMD sediment samples during the transformation experiment with and without As at pH 3.

Figure 5. Evolution of the XRD diffractograms of the synthetic analogue *Sch* (left panel) and natural AMD sample *POR3* (right panel), with and without As, during the transformation experiment. G – goethite; S – schwertmannite; Q – quartz.

Figure 6. EXAFS spectra ($k^3\chi(k)$ vs. k(Å^{-1})) for *Sch* and *POR3* samples, with and without As, during the transformation experiment (pH 3, As/Fe of 0.1). Solid lines are data and dotted lines are linear combination fits. $k^3\chi(k)$. Reference spectra used to do the linear combination fitting, i.e. goethite (*Goe*) and schwertmannite (*Sch*), are shown at the bottom of the figure.

Figure 7. Fraction of goethite as function of time at pH 3 in a suspension of: *Sch* (triangles), sediments sampled at *POR3* (rhomboid), *SchAs*, As/Fe = 0.1 (cross) and *POR3As*, As/Fe = 0.1 (circle).

Figure 8. Results of the transformation experiment in the presence of Fe(II) ions under anoxic conditions for the sample *POR3*. Left panels show the variation in the sulphate concentration in solution in the presence of 10 mM Fe(II) (filled symbols) and in the absence of Fe(II)

(empty symbols) at different pH values (Dashed line indicates the maximum sulphate release attending to the chemical composition of the sample). Right panels show the XRD diffractograms of the final solid collected after a 24 h incubation period in the presence of 10 mM Fe(II). G – goethite; S – schwertmannite; R – roemerite.

Figure 9. Evolution of Fe(II) concentration in solution and redox potential during the transformation experiment under anoxic conditions. Empty and filled symbols correspond to the Fe(II) concentrations at pH 6 and 7, respectively. Dashed and solid lines correspond to the Eh at pH 6 and 7, respectively.

Figure 10. Change in dissolved Fe(II) concentration as function of time after addition of 250 μM ascorbic acid to the suspension. The figure on the left shows data for reductive dissolution of synthetic schwertmannite at: pH = 3, As/Fe = 0 (black empty circle), pH = 3, As/Fe = 0.1 (grey filled circle), pH = 5, As/Fe = 0 (black empty square) and pH = 5, As/Fe = 0.1 (grey filled square). The reductive dissolution of sediments sampled at *POR3* are shown in the figure on the right at: pH = 3, As/Fe = 0 (black empty triangle), pH = 3, As/Fe = 0.1 (grey filled triangle), pH = 5, As/Fe = 0 (black empty rhomboid) and pH = 5, As/Fe = 0.1 (grey filled rhomboid).

Figure 1

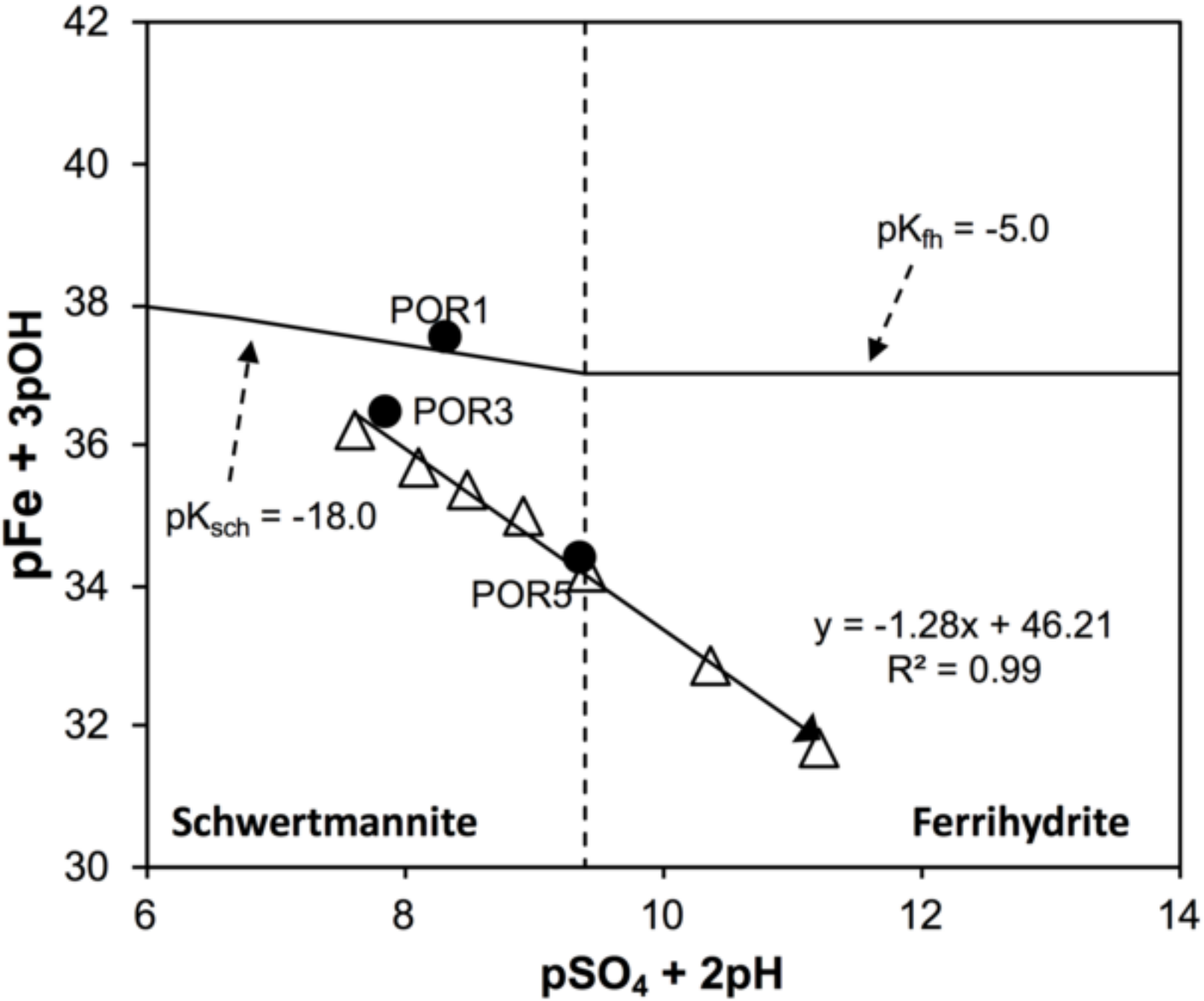

Figure 2

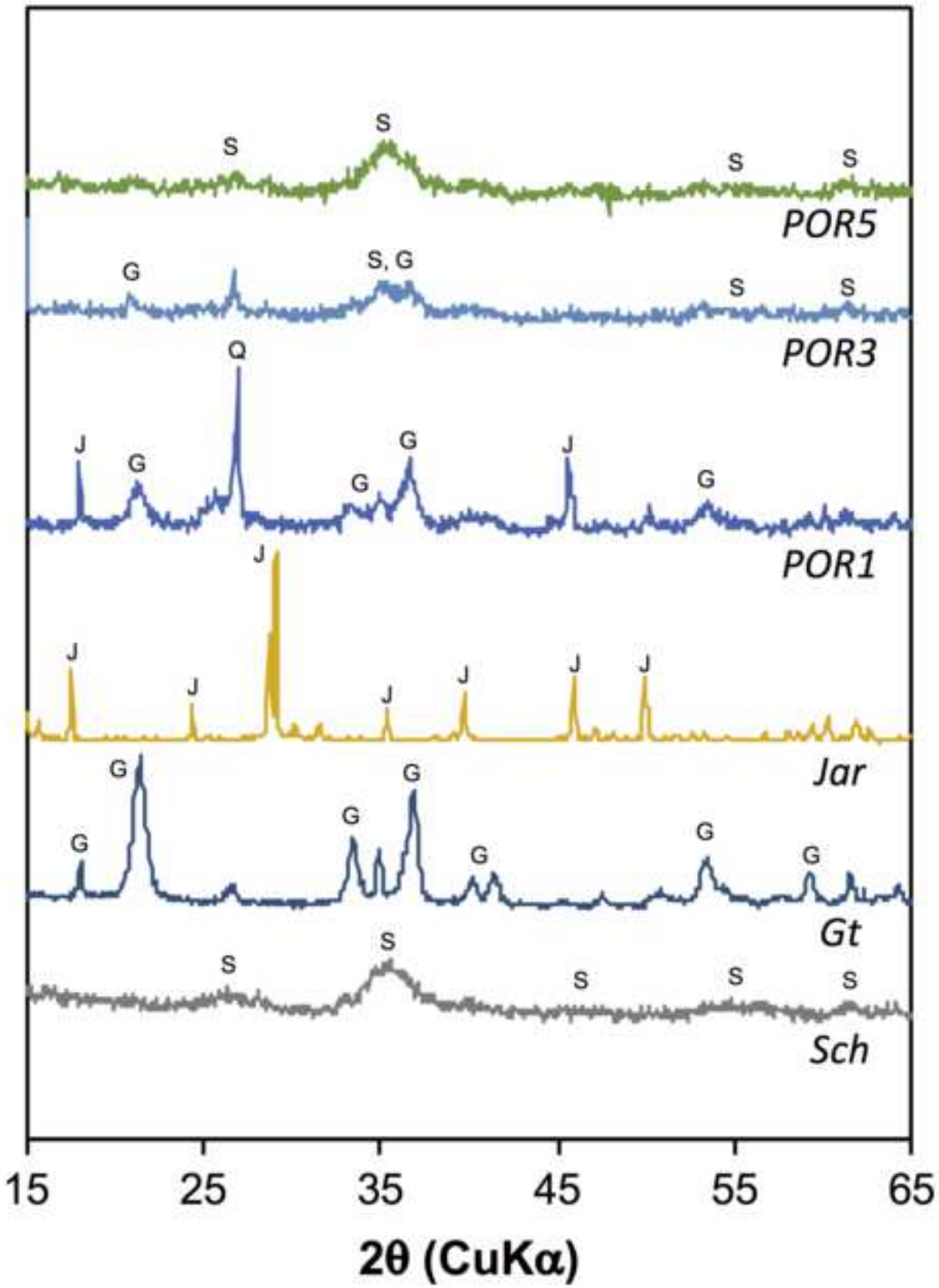

Figure 3

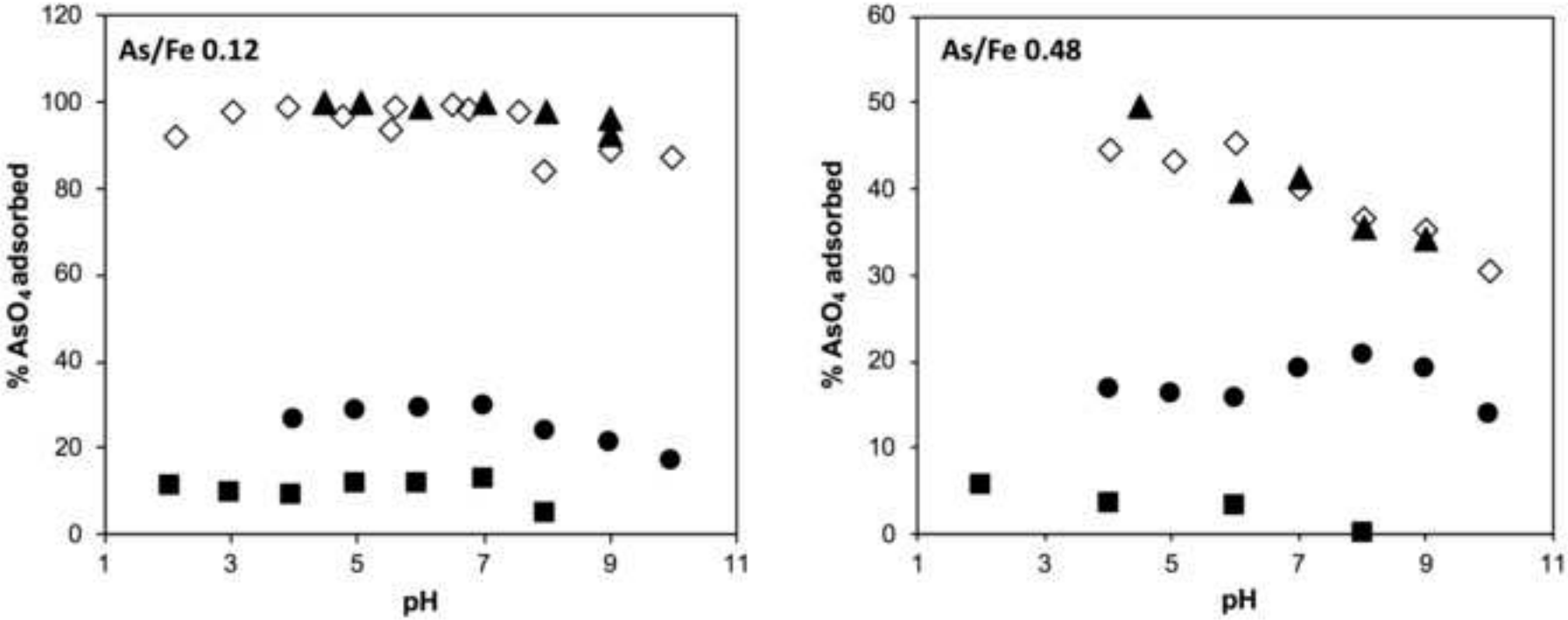

Figure 4

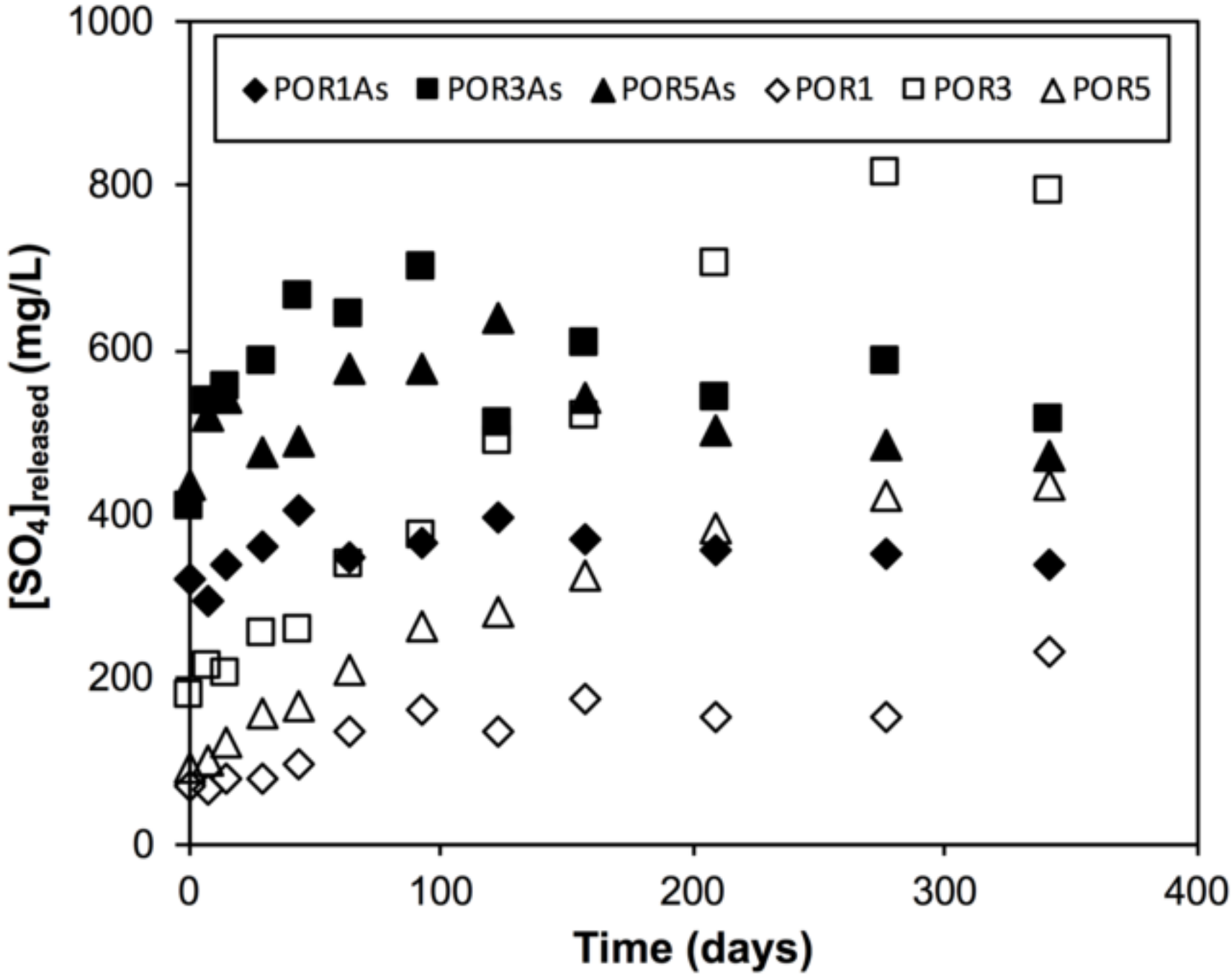

Figure 5

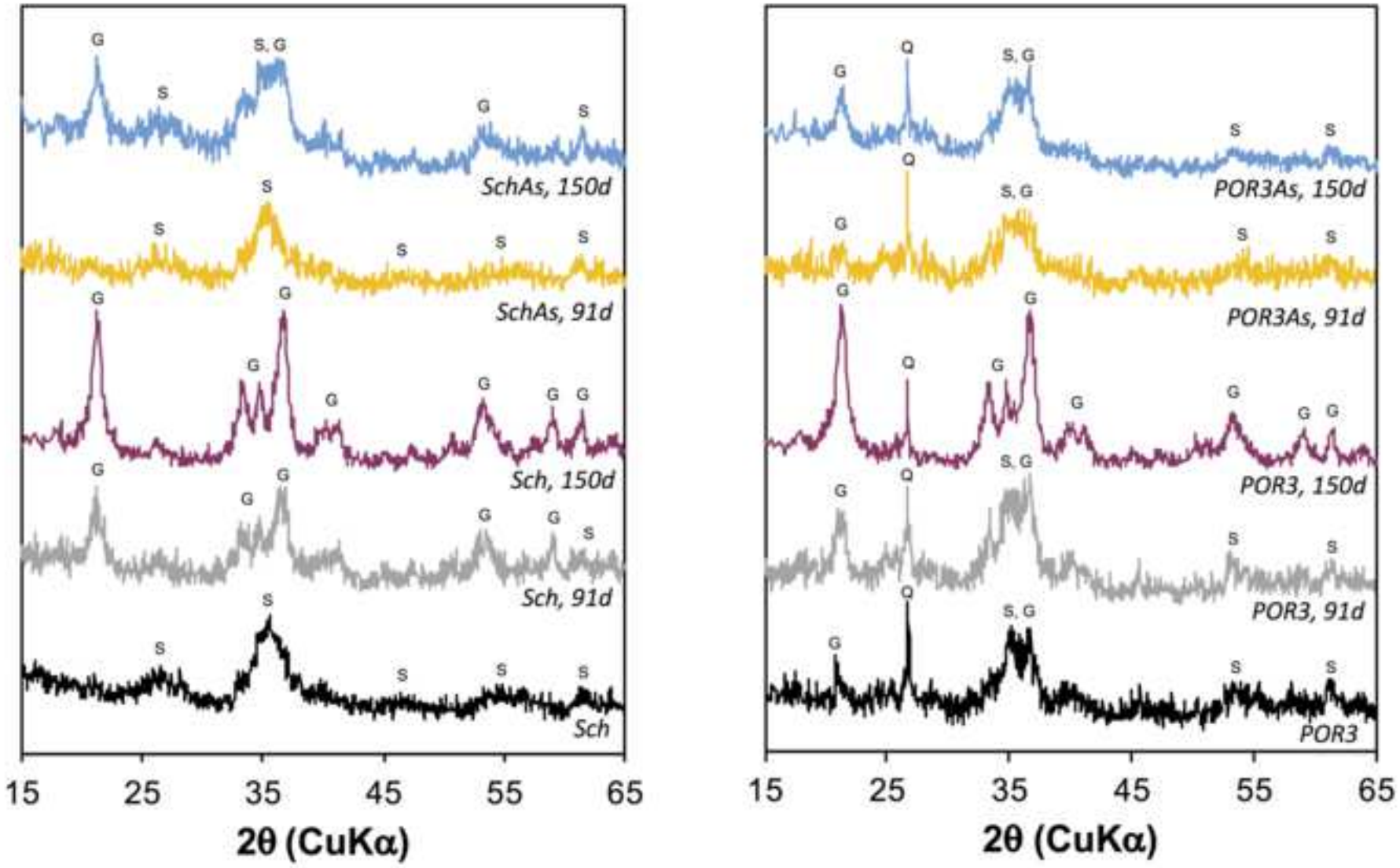

Figure 6

Click here to access/download;Figure;Figure 6.tiff

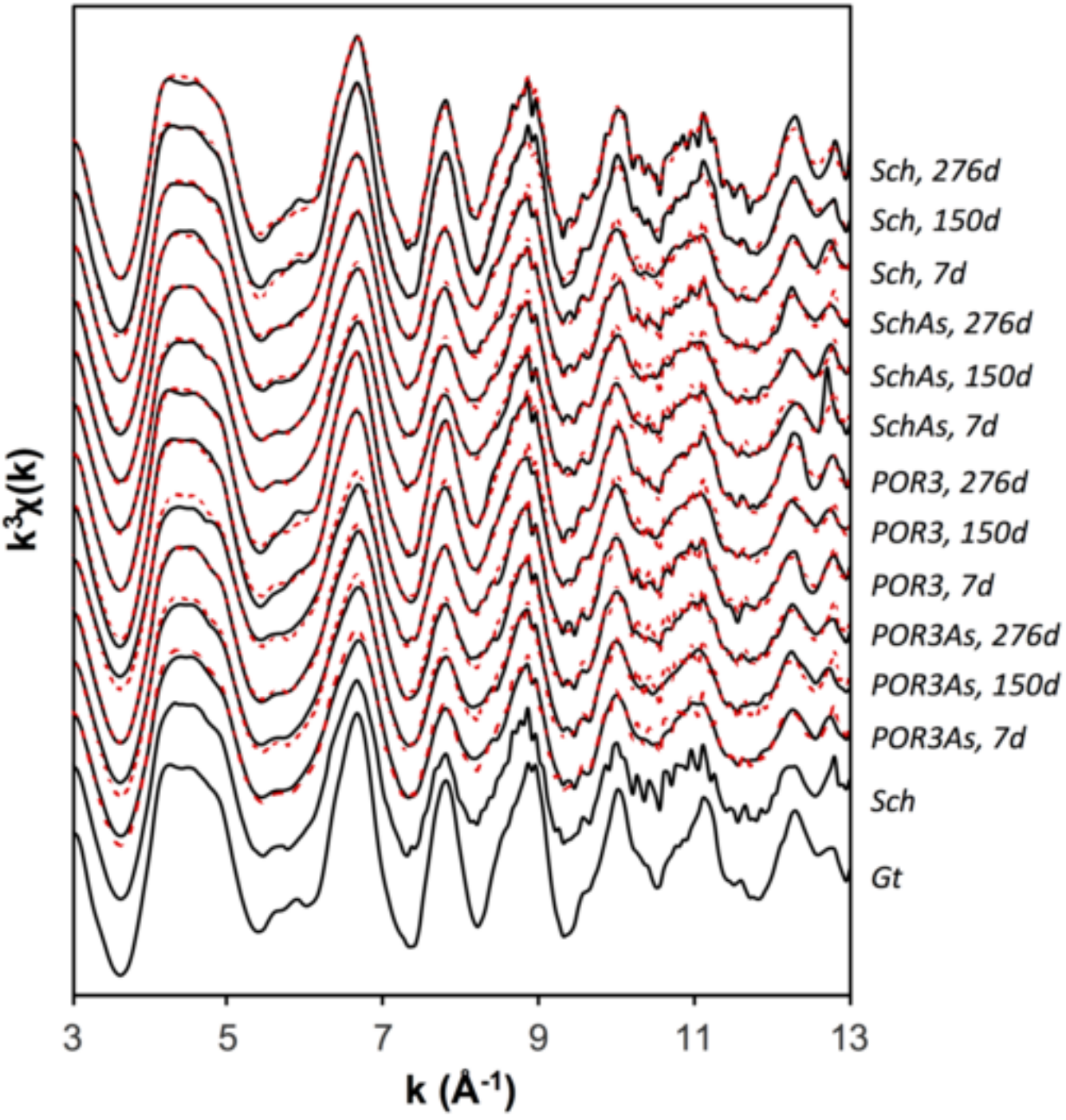

Figure 7

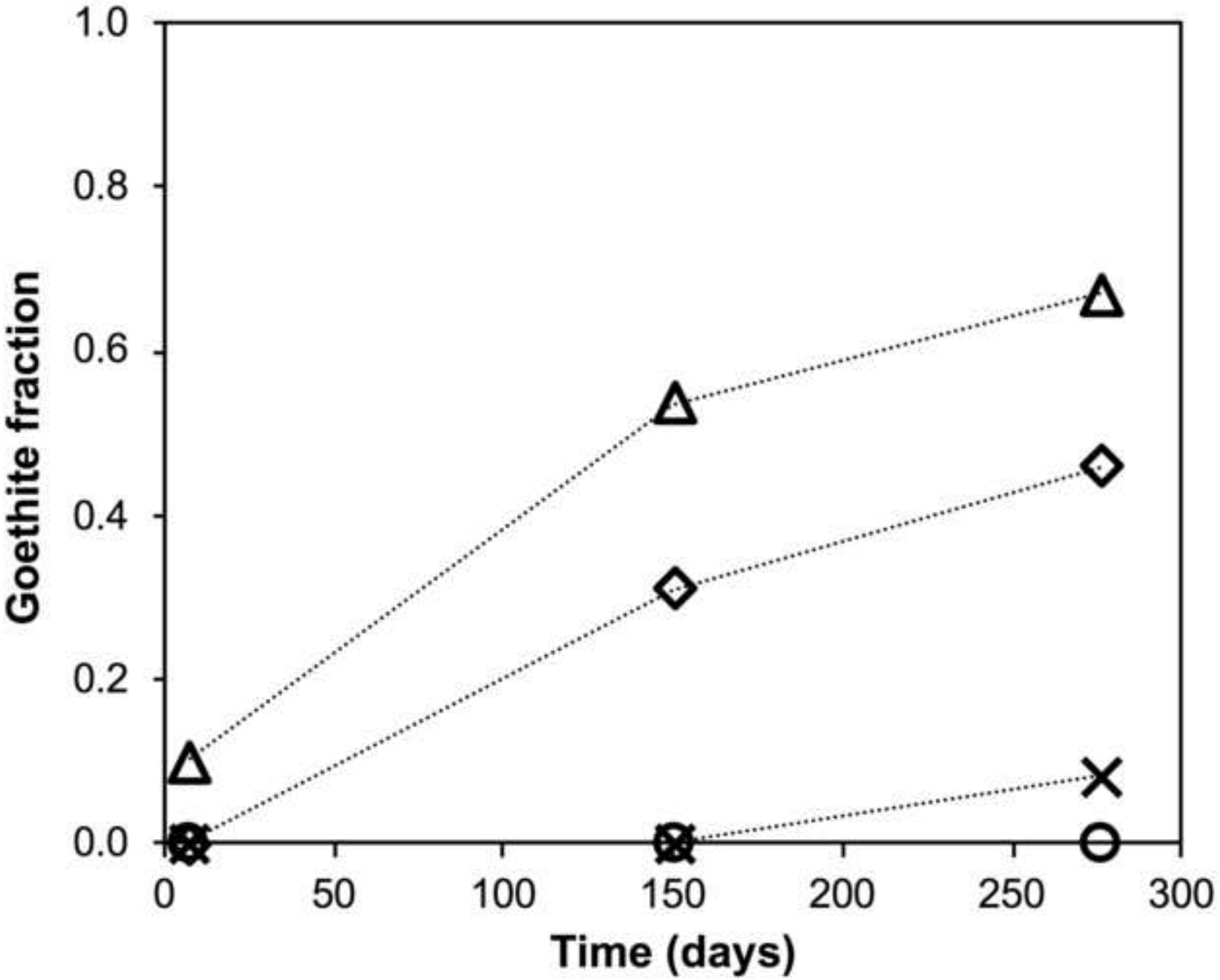

Figure 8

Click here to access/download;Figure;Figure 8.tiff

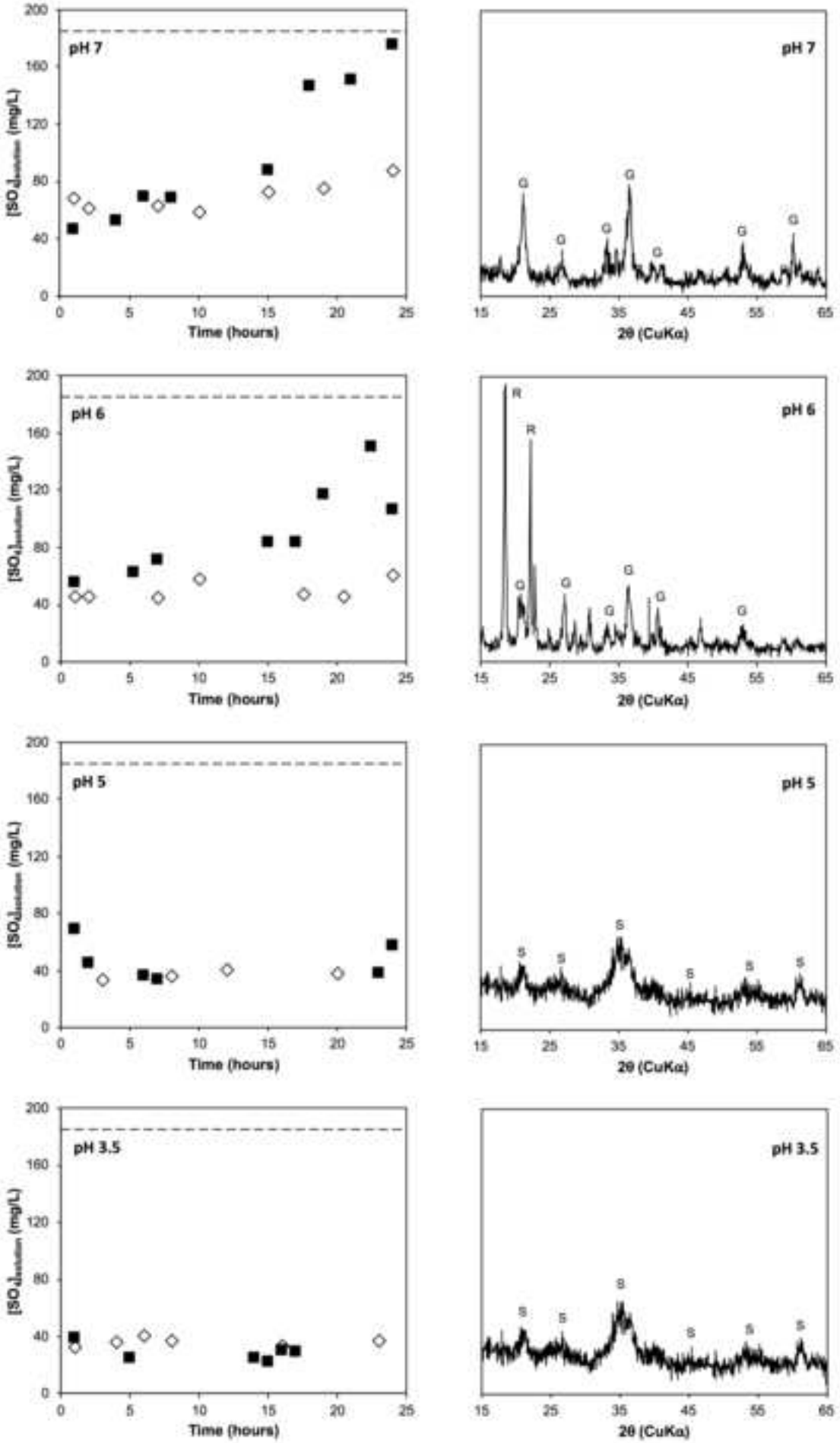

Figure 9

Click here to access/download;Figure;Figure 9.tiff

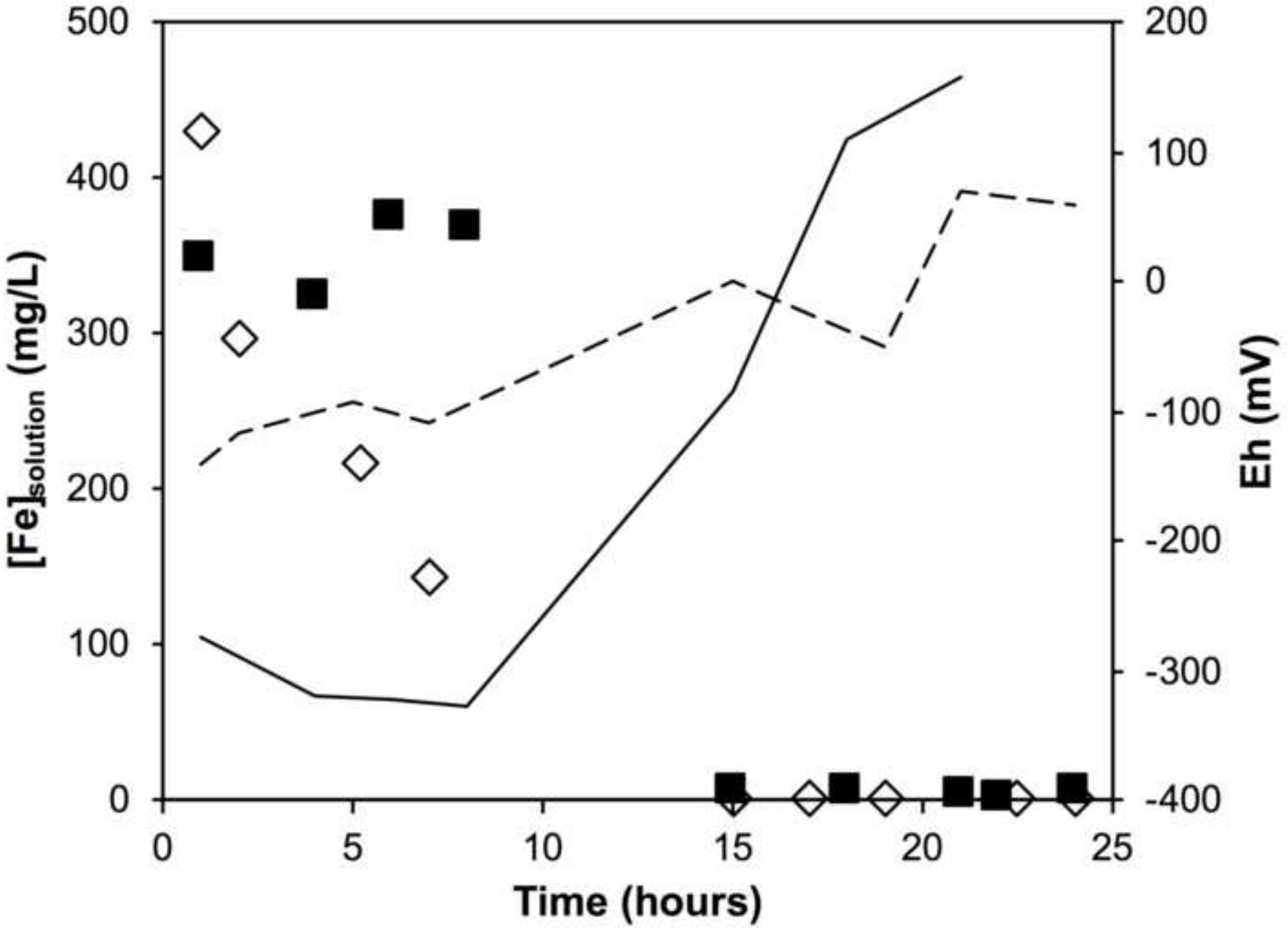

Figure 10

Click here to access/download;Figure;Figure 10.tiff

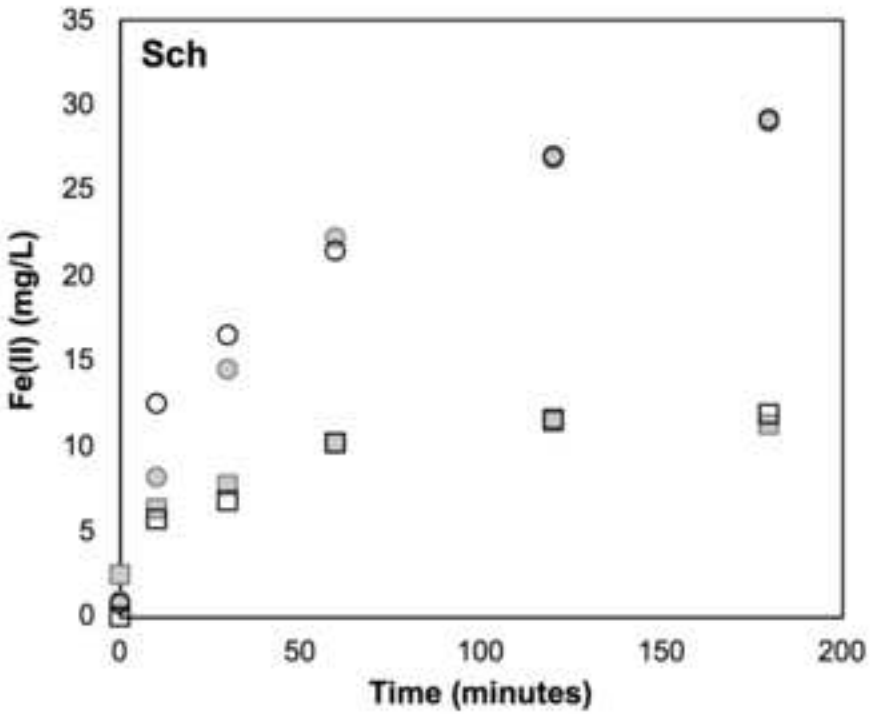

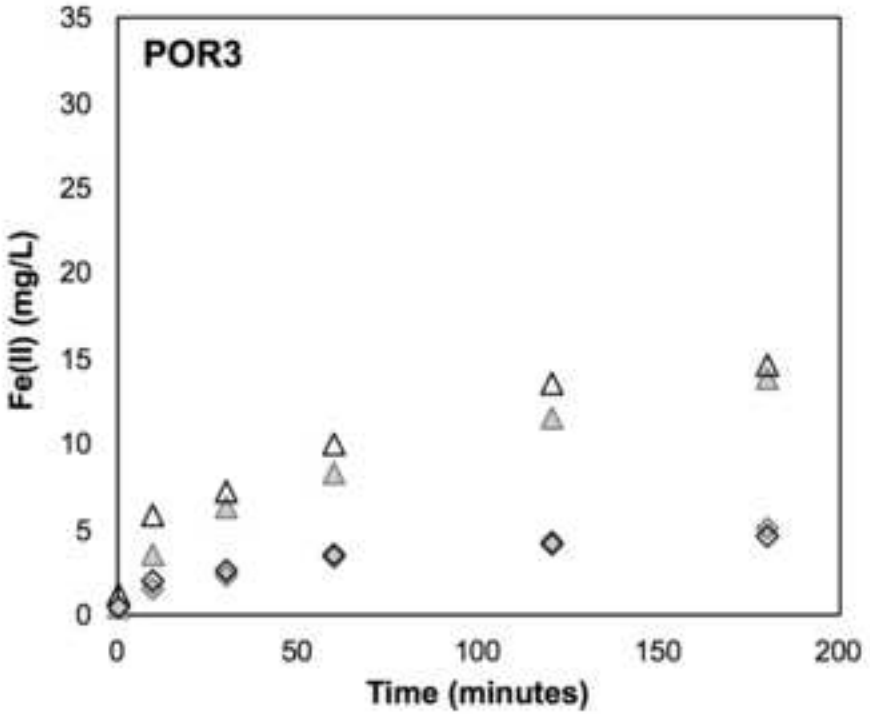

Juan Antelo: Investigation, Conceptualization, Methodology, Writing - original draft, Supervision

Sarah Fiol: Investigation, Conceptualization, Methodology, Writing - review & editing, Project administration, Funding acquisition

Ivan Carabante: Investigation, Conceptualization, Methodology, Writing - review & editing, Supervision, Funding acquisition

Arantxa Arroyo: Investigation, Methodology

Juan S. Lezama-Pacheco: Investigation, Formal Analysis

Natasha Josevska: Investigation, Methodology

Chloe Protopapa: Investigation, Methodology

Jurate Kumpiene: Project administration, Resources, Funding acquisition.